Available online at www.sciencedirect.com

SciVerse ScienceDirect

journal homepage: www.elsevier.com/locate/he

Analysis of Pt/C electrode performance in a flowing-electrolyte alkaline fuel cell

Fikile R. Brushett [a], *Matthew S. Naughton* [a], *Jia Wei Desmond Ng* [a], *Leilei Yin* [b], *Paul J.A. Kenis* [a,b,c,*]

[a] *Department of Chemical & Biomolecular Engineering, University of Illinois at Urbana-Champaign, Urbana, IL 61801, USA*
[b] *Beckman Institute for Advanced Science and Technology, University of Illinois at Urbana-Champaign, Urbana, IL 61801, USA*
[c] *Materials Research Laboratory, University of Illinois at Urbana-Champaign, Urbana, IL 61801, USA*

ARTICLE INFO

Article history:
Received 17 June 2011
Received in revised form
17 October 2011
Accepted 18 October 2011
Available online 12 November 2011

Keywords:
Alkaline fuel cell
Electrode characterization
X-ray micro-computed tomography
Microfluidic fuel cell
Carbonates

ABSTRACT

We characterize the performance of Pt/C-based electrodes under alkaline conditions using a microfluidic H_2/O_2 fuel cell as an analytical platform. Both anodes and cathodes were investigated as a function of electrode preparation procedures (*i.e.*, hot pressing, acclimatization) and fuel cell operating parameters (*i.e.*, electrolyte composition) via chronoamperometric and electrochemical impedance analyses. X-ray micro-computed tomography was employed to link electrode structure to performance. In addition, the flowing electrolyte stream is used to study the effects of carbonates on individual electrode and overall fuel cell performance. Our studies provide direct evidence that the performance of hydrogen-fueled room-temperature alkaline fuel cells (AFCs) is limited by transport processes to and from the anode primarily due to water formation. Furthermore, the presence of carbonate species in the electrolyte appears to impact only anode performance whereas cathode performance remains unchanged.

1. Introduction

For the widespread commercialization of present acidic polymer electrolyte membrane (PEM)-based fuel cell technologies to be realized, significant enhancements in durability and reductions in cost are needed [1,2]. Of late, alkaline fuel cells (AFCs) have received renewed interest because they may overcome some of the hurdles that hamper the commercialization of their acidic counterparts. Under alkaline conditions, the kinetics of the oxygen reduction reaction (ORR) on the cathode are enhanced leading to improved fuel cell energetic efficiency and reduced need for high loadings of precious metal catalysts, i.e., platinum (Pt) [3]. Furthermore, a wider range of materials are stable in alkaline media, compared to acidic media, facilitating the implementation of cheap non-noble metal catalysts, i.e., silver (Ag) cathodes and nickel (Ni) anodes, as well as other low-cost structural materials, i.e., Ni current collectors, which can significantly lower fuel cell costs [4]. Consequently, AFCs have significant promise as an alternative to acidic PEM-based fuel cells for low-temperature applications [5,6].

Traditional AFC configurations with stationary liquid electrolytes, typically concentrated potassium hydroxide (30–45 wt% KOH), have been applied successfully over many decades, for example in vehicular applications and in the NASA Apollo space program in the 1950s and 1960s [1,5,7,8].

* *Corresponding author*. Department of Chemical & Biomolecular Engineering, University of Illinois at Urbana-Champaign, Urbana, IL 61801, USA
E-mail address: kenis@illinois.edu (P.J.A. Kenis).

0360-3199/$ – see front matter Copyright © 2011, Hydrogen Energy Publications, LLC. Published by Elsevier Ltd. All rights reserved.
doi:10.1016/j.ijhydene.2011.10.078

The major technical concerns for these traditional AFCs are (i) electrode durability in highly caustic environments (*i.e.*, hydrophobicity losses), (ii) carbonate formation when oxidizing organic fuels directly, and to a lesser extent (iii) water management at the electrodes (anode flooding and cathode dry-out) [9]. Of particular importance is carbonate formation (CO_3^{2-}/HCO_3^-), which occurs when the hydroxyl ions (OH^-) present in the electrolyte react with carbon dioxide (CO_2) mainly from either organic fuel oxidation, or the environment in which the system operates (*e.g.*, air, tailpipe emissions from automobiles). In the presence of mobile cations, the carbonates can precipitate within the electrodes, where they damage and/or clog the microporous architecture, block electrocatalytic sites, and eventually reduce performance. Furthermore, carbonate formation reduces the OH^- concentration in the liquid electrolyte, thus lowering electrolyte conductivity and electrode reaction kinetics. Consequently, these traditional AFCs were mainly limited to applications where cost was not a concern, which allowed for the use of high purity hydrogen (H_2) and oxygen (O_2) gas streams with ultra-low CO_2 concentrations and no internal carbonate formation by definition, thus avoiding carbonate formation-related issues in the stationary electrolyte [7].

To alleviate carbonate and water management-related issues, AFCs with *circulating* electrolyte streams have been developed that exhibit improved performance and lifetime compared to AFCs with stationary electrolytes [4,9–12]. The flowing electrolyte improves heat and water management and facilitates carbonate removal, which results in CO_2 tolerance up to ~100 ppm [9]. While such flowing configurations prolong AFC lifetimes, the electrolyte solution must still be periodically replenished or replaced to maintain conductivity and prevent carbonate precipitation due to saturation over long operational lifetimes. To further extend lifetimes, modern liquid electrolyte-based AFCs also incorporate CO_2 scrubbers (*i.e.*, soda lime) at the air inlet. However, the circulating electrolyte system and scrubber are ancillary systems that increase both parasitic losses and device complexity. In addition, electrode durability in the caustic environment remains a challenge [9]. Leaking of concentrated electrolyte has also been cited as a consumer safety concern [4].

As an alternative to liquid electrolyte-based AFCs, novel alkaline anion exchange membrane (AAEM)-based fuel cells are being pursued because these membrane-based designs reduce system complexity and increase device robustness but still maintain the electrocatalytic advantages of operating under alkaline conditions [13–16]. Furthermore, AAEMs are less susceptible to carbonate precipitation because no mobile cations exist *within the membrane* enabling less stringent operating conditions such as direct air-breathing cathodes. Still, the presence of carbonate ions in or near the AAEM can adversely impact cell performance (*e.g.*, unfavorable pH gradients, reduced conductivity) particularly in the case of direct liquid AAEM-based fuel cells [17]. Also, carbonate precipitation is still possible in the presence of metal ions in the electrode structure or the reactant streams [2]. Over the past decade, research on AAEM technologies has led to dramatic enhancements in cell stability and membrane conductivity [18]; however, several key challenges remain such as high costs and insufficient performance and durability under fuel cell operating conditions, especially at elevated temperatures [13]. For example, AAEM-based fuel cells, like acidic PEM-based fuel cells, are hampered by membrane limitations, notably membrane conductivity and water management at the electrodes (anode flooding and cathode dry-out) [19].

Developing a better understanding of the complex electrochemical, transport, and degradation processes that govern the performance and durability of electrodes within operating fuel cells is critical to designing the robust, inexpensive configurations that are required for commercial introduction [20–23]. However, detailed *in-situ* investigations of individual electrode processes are complicated by other factors such as water management, uneven performance across electrodes, and temperature gradients. Indeed, too many processes are interdependent on the same few variable parameters, necessitating analytical platforms with high degrees of freedom. To this end, we have developed a pH-flexible microfluidic H_2/O_2 fuel cell with a flowing electrolyte stream instead of a stationary membrane (Fig. 1) [24–26]. The flowing electrolyte (i) minimizes adverse fuel cell system limitations, *i.e.* water management, (ii) enables independent control of electrolyte parameters (*i.e.*, pH, composition) and consequently local electrode environments, and (iii) allows for *in-situ* studies of single electrode performance via an external reference electrode [25,27]. Previously, we have demonstrated the utility of this analytical platform to characterize the performance of Pt/C and Ag/C-based cathodes under alkaline conditions [24]. This platform can be used to systematically probe the key structural factors and operating conditions that govern the performance and durability of individual electrodes within operating AFCs. Such studies will be critical in guiding the development of robust and cost-effective liquid- and membrane-based AFC systems.

Here, we use the microfluidic H_2/O_2 fuel cell to identify performance-limiting factors for room-temperature H_2-fueled AFCs. The performance of Pt/C-based electrodes, both anodes and cathodes, is investigated as a function of electrode preparation protocols (*i.e.*, hot-pressing, acclimatization) and cell operating parameters (*i.e.*, electrolyte composition). In addition, we analyze the impact of carbonate species on individual electrode and overall fuel cell performance by introducing the contaminants via the flowing electrolyte stream.

2. Experimental

2.1. Gas diffusion electrode preparation

For each electrode, a catalyst ink was prepared by mixing 8 mg Pt/C (50% mass on Vulcan carbon, E-Tek), 5.33 mg polytetrafluorethylene powder (PTFE, Aldrich) as the hydrophobic catalyst binder, 200 μL Millipore water (18.2 MΩ) and 200 μL isopropyl alcohol. Previously, the optimal weight percentage of PTFE to the total weight of the PTFE/catalyst mixture within the catalyst ink was determined to be 40 wt% [24]. This catalyst ink was sonicated (Branson 3510) for 1 h to obtain a uniform mixture, which was then painted onto the microporous side of a Toray carbon paper gas diffusion layer (GDL, EFCG "S" type electrode, E-Tek). The GDLs consist of two

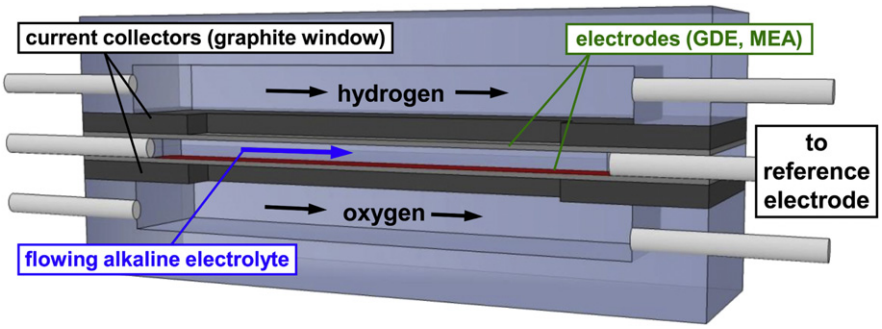

Fig. 1 – Microfluidic H_2/O_2 fuel cell with an independently-controlled flowing alkaline electrolyte stream separated from gaseous hydrogen and oxygen streams by two gas diffusion electrodes (GDEs) with the catalyst-coated side interfaces with the electrolyte. Two graphite windows function as current collectors on either side of the GDEs and polycarbonate flow chambers for reactant delivery. An external reference electrode is placed in an electrolyte collection beaker for monitoring individual electrode performance characteristics.

distinct carbonaceous layers: a microporous layer comprised of a mixture of carbon particles and PTFE mixture and a macroporous layer comprised of carbon fibers, PTFE, and a binder [28]. The GDE was sintered under a nitrogen (N_2) atmosphere at 330 °C for 20 min in a preheated tube furnace (Lindberg/Blue M Laboratory Furnace) [29]. Then, certain fabricated GDEs were hot pressed (Carver 3851-0) at a pressure of ~340 psi (~2344 kPa) and a temperature of ~125 ± 10 °C for 5 min [29]. The geometric GDE surface area was 4 cm^2 (4 (L) × 1 (W) cm^2) with 1 cm^2 exposed during fuel cell testing. For all the electrodes studied, the total catalyst loading was 2 mg Pt/C/cm^2 with a metal loading of 1 mg Pt/cm^2.

2.2. *X-ray micro-computed tomography (MicroCT)*

X-ray micro-computed tomography (MicroCT) is an X-ray absorption method that identifies different phases/elements as well as heterogeneous densities via variations in X-ray attenuation through the sample, in this case a GDE [30]. The sample is rotated in the X-ray beam during data collection. 2D radiographic cross-sectional image stacks and 3D tomographic virtual models of the GDE can be computed from the raw data to provide detailed information about layer thickness, internal architecture, and species location. Fig. 2a shows a schematic of the MicroCT experimental set-up. All GDE imaging was performed using a Xradia Micro-XCT 200 system. This instrument uses a cone beam reconstruction method where a micro-focus X-ray tube (Hamamatsu) is used as the X-ray source and a variable-magnification scintillator with a 4-megapixel thermoelectrically-cooled charge-coupled device (CCD) camera (Andor) as the X-ray collector. A small section, approximately 1.5 (W) × 5 (L) mm^2, was cut from each GDE and mounted in a Kapton tube (0.0641 in inner diameter, 0.0125 in wall thickness, Small Parts) which functions as an X-ray transparent sample holder. The sample was placed on a rotating stand within the MicroCT system between the X-ray source and the X-ray camera. The X-ray source was at a potential of 44–45 kV and a current of 60–66 μA. The scintillator magnification used was 20×. During imaging, the sample was rotated stepwise over 180° to capture 365 to 369 projection images called shadow-graphs. From these shadow-graphs, 2D image stacks (in the xy, xz, and yz planes), and 3D tomographic volumes are generated. The image stacks consisted of 800 images with a resolution of 1.078 μm/pixel. The virtual models had a resolution of 1.252 μm^3/voxel where a voxel is a volumetric pixel.

Xradia 3D viewer software was used to perform data analysis on the 2D image stacks. To determine the average

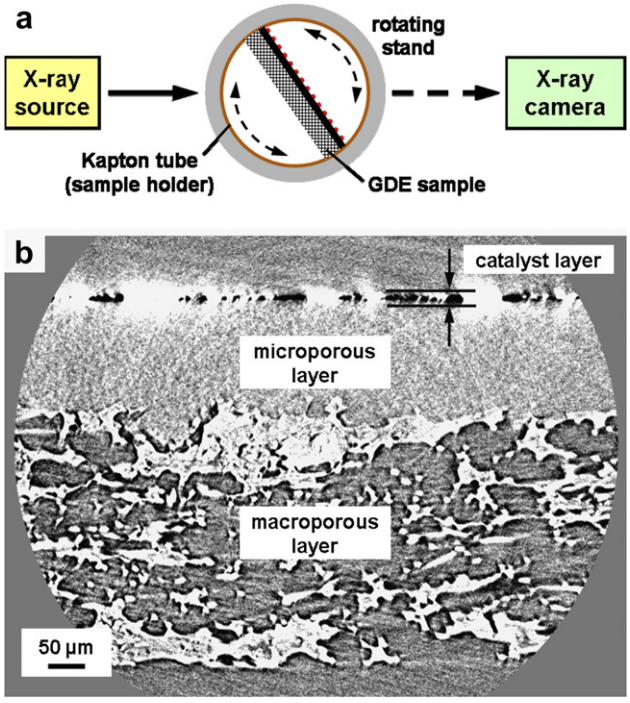

Fig. 2 – (a) Schematic of MicroCT set-up: the GDE sample is rotated stepwise over 180°. (b) A representative *xz*-plane radiographic image of a hot-pressed GDE which consists of a Pt/C-PTFE catalyst layer hand-painted on a GDL (EFCG "S" type electrode, E-tek). Electrode hot-pressing conditions were P = 340 psi and T = 125 ± 10 °C for 5 min. Electrode loading was 2 mg Pt/C/cm^2 (1 mg Pt/cm^2). Image is #100 of an 800-image stack and the resolution is 1.078 μm/pixel.

layer thickness (z-direction) of each sample, the through-plane (xz-plane) cross-sectional images were analyzed. The z-direction may also be thought of the depth of the sample. A representative 2D image is shown in Fig. 2b. The thickness (y-direction) of each of these images is one pixel which corresponds to the image resolution. Each layer thickness measurement was taken across a 2D xy-plane grid with 100 μm between each point. This corresponded to 49 data points across each GDE sample. Prior to calculating the mean and standard deviation, a quartile technique is employed to eliminate extreme outliers from the data set.

2.3. *Fuel cell assembly and testing*

Fig. 1 shows a cross-sectional schematic of the microfluidic fuel cell configuration. Two GDEs, an anode and a cathode, were placed on opposite sides of a 0.15-cm thick polymethylmethacrylate (PMMA) sheet, such that the catalyst-covered sides interfaced with the 3-cm long and 0.33-cm wide precision-machined window in the PMMA. The geometric surface area used to calculate current and power density is 1 cm^2 (based on the electrolyte channel length and width). The window has an inlet and an outlet on either side such that the aqueous electrolyte flows between the electrodes. Two 0.1-cm thick graphite plates with access windows (3.8 (L) × 0.7 (W) cm^2) are placed on the outside of the GDEs and serve as current collectors. The reactant gas flow chambers (5 (L) × 1 (W) × 0.5 (H) cm^3) were precision-machined into polycarbonate sheets. The multilayer assembly was held together using binder clips (Highmark). Prior to experimentation, the fuel cell assembly was leak tested by flowing deionized water through the fluidic chamber for several minutes.

Fuel cell experiments were conducted using General Purpose Electrochemical Software (GPES, EcoChemie) controlled by a potentiostat (Autolab PGSTAT-302N, EcoChemie) at room temperature. H_2 and O_2 gas (laboratory grade, S.J. Smith) are each fed at a flow rate of 50 sccm [25]. Electrolyte flow rates were varied from 0.0 to 0.9 mL/min using a syringe pump (2200 PHD, Harvard Apparatus). Potassium hydroxide (KOH, Mallinckrodt, 88%, balance of H_2O), sodium hydroxide (NaOH, Fisher Chemical, 98.2%), and potassium carbonate (K_2CO_3, Fisher Chemical, 99.8%) were used as aqueous alkaline electrolytes. Once the gas and liquid streams were introduced, the fuel cell was held at open circuit potential (OCP) for 5 min to ensure that the cell potential stabilized prior to testing. Fuel cell polarization curves were obtained by steady-state chronoamperometric measurements at different cell potentials. After exiting the fuel cell, the aqueous electrolyte stream collects in a beaker. The anode and cathode polarization losses are independently measured using multimeters (15 XP Meterman, 87 III Fluke, or 179 Fluke) by placing a reference electrode (Ag/AgCl in saturated NaCl, BASi) in the collection beaker. No potential drop is observed along the plastic tubing (Cole Parmer, 1.57 mm ID) connecting the fuel cell and the reference electrode [27]. The open circuit potential of the Pt/C anode, exposed to 50 sccm H_2, was used to calibrate the reference electrode to the reversible hydrogen electrode (RHE) scale.

Electrochemical impedance spectroscopy (EIS) measurements were performed on the fuel cell using a Frequency Response Analyzer (FRA, EcoChemie) module controlled by another potentiostat (Autolab PGSTAT-30, EcoChemie) at room temperature. The spectra were recorded in constant voltage mode by decreasing frequencies from 10 kHz to 30 mHz at 9 points/decade. The modulating voltage was 10 mV root mean squared. Impedance measurements were performed at a cell potential of 0.4 V, coinciding with the peak power density of the cells studied. The high frequency *x*-axis intercepts represent the internal cell resistance (R_{cell}) which includes both electrolyte solution resistance and component contact resistances [31]. The individual semi-circular features in the Nyquist plots were fitted with parallel RC equivalent circuits replacing the pure capacitive elements (C_{dl}) with constant phase elements (C_{cpe}) to describe the porous nature of the GDE [19]. The diameter of medium-frequency semi-circular feature represents the charge-transfer resistance (R_{ct}) associated with the Faradaic processes on the fuel cell electrodes. The low-frequency features represent the effects of mass transport limitations on fuel cell processes [32].

3. Results and discussion

Using a microfluidic H_2/O_2 fuel cell as an analytical platform, the performance of Pt/C-based anodes and cathodes is characterized in alkaline media over a wide range of experimental conditions. First, the effects of electrode preparation, specifically acclimatization and hot-pressing, on performance are investigated via electrochemical and MicroCT studies. Second, the impact of electrolyte composition, specifically KOH concentration and carbonate content, on performance are studied via fuel cell and electrochemical impedance analyses.

3.1. *Effects of acclimatization on electrode performance*

Prior to initial use, most fuel cell systems require a “break-in” period of acclimatization for performance to stabilize [33,34]. After fabrication, all the GDEs demonstrated significant hydrophobicity due to the presence of excess PTFE on the surface preventing catalyst wetting. *In-situ* cyclic voltammetry was performed on the electrodes within the microfluidic fuel cell to remove excess binder from the three-phase interface. Studies were conducted by flowing gaseous N_2 and H_2 streams (at 50 sccm each) over the two electrodes to create a working electrode, which function as an anode, and a dynamic hydrogen electrode (DHE), which functions as a cathode as well as a reference electrode. Because the hydrogen-cathode functions as a stable reference electrode against which the anode polarizes, a flowing acidic electrolyte, 0.5 M H_2SO_4 (GFS Chemicals), was used since hydrogen oxidation/reduction kinetics are faster under acidic conditions than under alkaline conditions [35]. Prior to cycling, the electrodes were flushed for 5 min to remove any O_2. Acclimatization was performed by cycling the anode between 0.05 and 1.15 V vs. DHE at a scan rate of 0.5 V/s in 10 min intervals. After each interval, the electrode assembly was inverted such that the working electrode became the counter/reference electrode and the counter/reference electrode became the working electrode. The second electrode was then run under identical conditions.

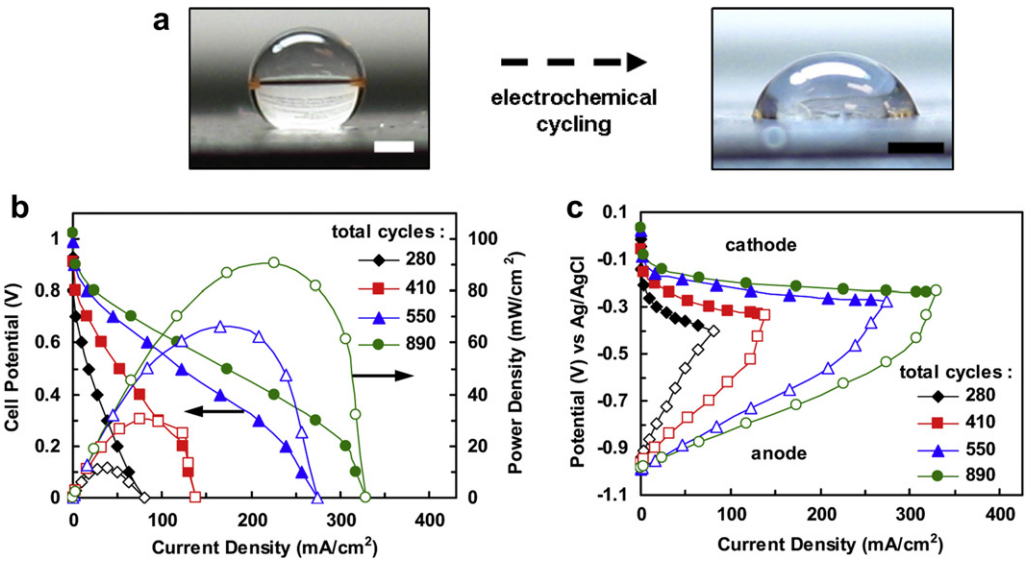

Fig. 3 – (a) Digital photographs of water droplet wetting on the Pt/C-PTFE electrode surface before and after *in-situ* cyclic voltammetry in a microfluidic H_2/O_2 fuel cell. (b) Representative polarization and power density curves after different numbers of electrochemical cycles. (c) Corresponding representative anode and cathode polarization curves. In all studies, H_2/O_2 flow rates were 50 sccm each, electrode loadings were 2 mg Pt/C/cm^2 (1 mg Pt/cm^2), and experiments were performed at room temperature. Both scale bars represent 1 mm.

After a cycle set was completed, both electrodes were removed from the microfluidic fuel cell, rinsed with Millipore water (18.2 MΩ) to remove any residues, and dried under a laboratory hood. Electrode performance was then investigated in the re-assembled microfluidic H_2/O_2 fuel cell operated with 1 M KOH flowing at 0.6 mL/min.

Fig. 3 shows alkaline microfluidic H_2/O_2 fuel cell performance as a function of electrode acclimatization cycles. Prior to cycling, the extreme electrode surface hydrophobicity coupled with the PMMA channel hydrophilicity leads to electrolyte plug or slug flow behavior in the microfluidic channel in that the electrolyte wets the channel sidewalls but not the electrode surfaces. Consequently, initial fuel cell testing (at 0 cycles) was not possible. As electrochemical cycling removed excess PTFE, electrode surface hydrophilicity increased as observed by the increasing contact angle of a water droplet on the surface (Fig. 3a). As wetting increased, fuel cell performance also dramatically improved. As shown in Fig. 3b, fuel cell peak power densities of 11.4, 30.4, 66.4, and 90.4 mW/cm^2 were observed after 280, 410, 550, and 890 electrode cycles, respectively. Furthermore, fuel cell open circuit potentials (OCPs) of 0.93, 0.91, 0.99, and 1.02 V were observed after 280, 410, 550, and 890 cycles, respectively. No further enhancements were observed with additional cycling. Fig. 3c shows that the improved surface wetting enhances individual electrode performance by facilitating reactant transport to the catalytic sites, in this case water to the cathode and hydroxyl ions to the anode. Additional cycling was limited to prevent the electrode from becoming too hydrophilic, which would lead to catalyst layer flooding and reduce cell performance. Under these operating conditions, fuel cell performance is limited by the low hydroxyl ion concentration in the electrolyte (1 M KOH), which not only leads to ohmic losses due to low conductivity but also to anodic mass transport limitations because the rate of hydroxyl replenishment of the depletion boundary layer is insufficient (water formation on the anode). These effects are discussed in Section 3.3 and also in a previous publication [25]. Similar individual electrode and overall cell behavior were observed by Zeng *et al.* in a H_2/O_2 fuel cell with AAEMs of varying thicknesses and an *in-situ* Pd–Pt reference electrode [36]. The effects of KOH concentration on fuel cell performance are detailed in Section 3.4.

3.2. *Effects of hot-pressing on electrode performance*

For both liquid- and membrane-based fuel cells, electrode and membrane-electrode assembly (MEA) hot-pressing is intended to compact the layers together to minimize electrical contact resistances and to avoid delamination between interfacing layers [4,24,29,37]. However, over-compression of, and uneven pressure distribution across GDEs can damage the intricate electrode microstructure leading to losses in porosity and hydrophobicity and consequently to reductions in performance and durability [2,38,39]. MicroCT analysis enables the detailed analysis of the effects of hot-pressing on the GDL structure in a quantitative fashion. As shown in Table 1, hot-pressing ($P = 340$ psi, $T = 125 \pm 10$ °C) leads to a slight reduction in total GDL thickness by 31 ± 23 μm, primarily due to compression of the porous carbon fiber layer. Hot-pressing had a minimal effect on the catalyst layer thickness (not shown).

Next we investigated the effects of hot-pressing on the electrode performance in an alkaline microfluidic H_2/O_2 fuel cell operated at varying flow rates of 3 M KOH. The higher KOH concentration addresses the electrolyte-based transport

Table 1 – Comparative layer thickness analyses before and after hot-pressing GDLs via MicroCT imaging. Values for each GDL (EFCG "S" type electrode, E-tek), were obtained by measuring and averaging the layer thickness at 49 different points across the GDL sample.

Layer thickness	Non hot-pressed (Non-HP)	Hot-pressed(HP)
Hydrophobized carbon	114 ± 14 μm	109 ± 14 μm
Porous carbon fiber	358 ± 20 μm	334 ± 15 μm
Total GDL	473 ± 20 μm	442 ± 12 μm

limitation alluded to in Section 3.1 and enables access to higher current density regimes where electrode-based limitations may be studied. Two different electrode configurations were investigated: a hot-pressed (HP) anode with a non hot-pressed (non-HP) cathode (HP anode/non-HP cathode) and a non-HP anode with a HP cathode (non-HP anode/HP cathode). As individual electrode performance may be measured in the microfluidic fuel cell, the effects of hot-pressing of each electrode can be analyzed by inverting the electrode configuration between experiments. Fig. 4 shows the performance of the fuel cell operated with the two electrode configurations, HP anode/non-HP cathode and non-HP anode/HP cathode, as a function of electrolyte flow rate (0.0, 0.3, 0.6, and 0.9 mL/min) at 3 M KOH. Fig. 4a shows representative polarization and power density curves of the two fuel cell configurations operated at 0.3 mL/min. While the open circuit potentials and peak power densities are near identical for each configuration, the HP anode/non-HP cathode configuration is mass transfer limited at higher current densities. The corresponding individual electrode polarization curves indicate that anode mass transport effects, specifically water removal, limit its performance (Fig. 4b). The HP and non-HP cathodes show near identical performances suggesting that hot-pressing does not significantly impact cathode performance.

Further performance analyses of peak power density (Fig. 4c) and maximum current density (Fig. 4d) at varying electrolyte flow rates (0.0, 0.3, 0.6, and 0.9 mL/min) also demonstrate the effects of hot-pressing electrodes. For both configurations, the flowing electrolyte leads to improved performance as compared to the static electrolyte. However, the fuel cell performance appears to be independent of flow rate between 0.3 and 0.9 mL/min. The performance enhancement associated with a flowing electrolyte stream, again as opposed to a static electrolyte, is due to improved internal water management, specifically water removal from the anode surface. Under static conditions (0.0 mL/min), fuel cells operated with a non-HP anode/HP cathode configuration

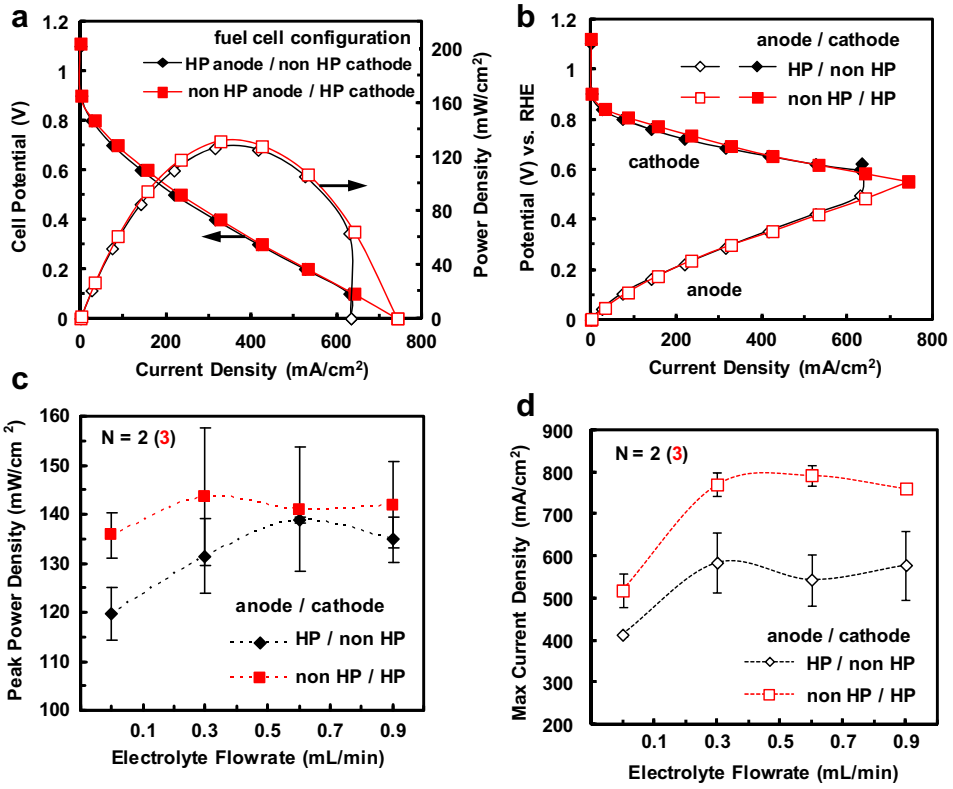

Fig. 4 – The two alkaline microfluidic H_2/O_2 fuel cell configurations studied at 3 M KOH are: HP anode/non-HP cathode (diamonds) and non-HP anode/HP cathode (squares). (a) Representative polarization and power density curves for fuel cells operated at 0.3 mL/min. (b) Corresponding anode and cathode polarization curves. (c) Peak power density ($N = 3$) and (d) maximum current density of the two fuel cell configurations as a function of electrolyte flow rate ($N = 2$ or 3). Error bars represent a standard deviation in either direction from the average cell power density at each flow rate. In all studies, H_2/O_2 flow rates were 50 sccm each, electrode loadings were 2 mg Pt/C/cm² (1 mg Pt/cm²), and experiments were performed at room temperature.

outperform those operated with a HP anode/non-HP cathode configuration in terms of both peak power density and maximum current density. With a flowing electrolyte, similar peak power densities are observed for both configurations (Fig. 4c); however, at maximum current densities (Fig. 4d), the non-HP anode/HP cathode fuel cell configuration outperforms the HP anode/non-HP cathode fuel cell configuration, as apparent from both Fig. 4a and b. At this point, large quantities of formed water must be removed rapidly from the anode necessitating optimal transport processes not only at the electrolyte–electrode interface but also within the GDE structure. These results suggest that hot-pressing adversely affects water management within the electrodes because non-HP anodes outperform HP anodes.

For all studies, cathode performance was both flow rate and hot-pressing independent. This independence is because internal electrode water management is not a significant concern as water is a reactant in the alkaline oxygen reduction reaction. Moreover, as the electrolyte is mostly water, increasing the flow rate has only a minimal effect on reactant diffusion to the cathode surface. Also, no catalyst delamination or flaking was observed suggesting that hot-pressing is not necessary for this purpose. Thus, hot-pressing appears to have negative effects on water management processes (transport and balance) within the GDE architecture which are likely due to changes in porosity as well as shifts in layer hydrophobicity. These *in-situ* results are further supported by previously reported *ex-situ* studies by Bazylak *et al.* on the effects of compression on GDL microstructure and water management [39]. The combined use of MicroCT and microfluidic fuel cells to analyze the effects of compression on individual electrode performance will be the subject of a future publication.

3.3. *Effects of KOH concentration on electrode performance*

Next, we studied the effects of electrolyte concentration (1, 3, 5, 7, and 9 M KOH) on individual electrode and overall fuel cell performance. Based on the results described in the previous section, we performed all subsequent experiments with a non-HP anode/HP cathode fuel cell configuration, operated at a flow rate of 0.3 mL/min. Determining the optimum KOH concentration in a liquid electrolyte-based AFC involves consideration of the tradeoffs between kinetics, conductivity, and viscosity, which all change as a function of concentration. Fig. 5a shows the polarization and power density curves for a microfluidic fuel cell operated with KOH concentrations of 1–9 M. The fuel cell generated peak power densities of 83.6, 111.6, 110.4, 95.4, and 76 mW/cm^2 for 1, 3, 5, 7, and 9 M KOH, respectively. As highlighted in Section 3.1, at 1 M KOH, fuel cell performance is limited by anode performance due to lower hydroxyl ion concentrations. Consequently, at low KOH concentrations, the anode performance is limited by the availability of hydroxyl ions. Optimal performance, in terms of peak power density, is observed at 3 and 5 M KOH. However, as concentration increases above 3 M KOH, cell performance lowers despite the increase in electrolyte conductivity, which peaks at 7 M, especially at low cell potentials (high current densities). Individual electrode polarization curves reveal that several processes lead to the reduced performance at higher concentrations (Fig. 5b). At higher KOH concentrations, reduced anode and cathode performances are observed due to increased solution viscosity which hampers transport processes, as described previously [40]. This effect is especially pronounced at higher current densities where anode performance is limiting due to mass transport losses.

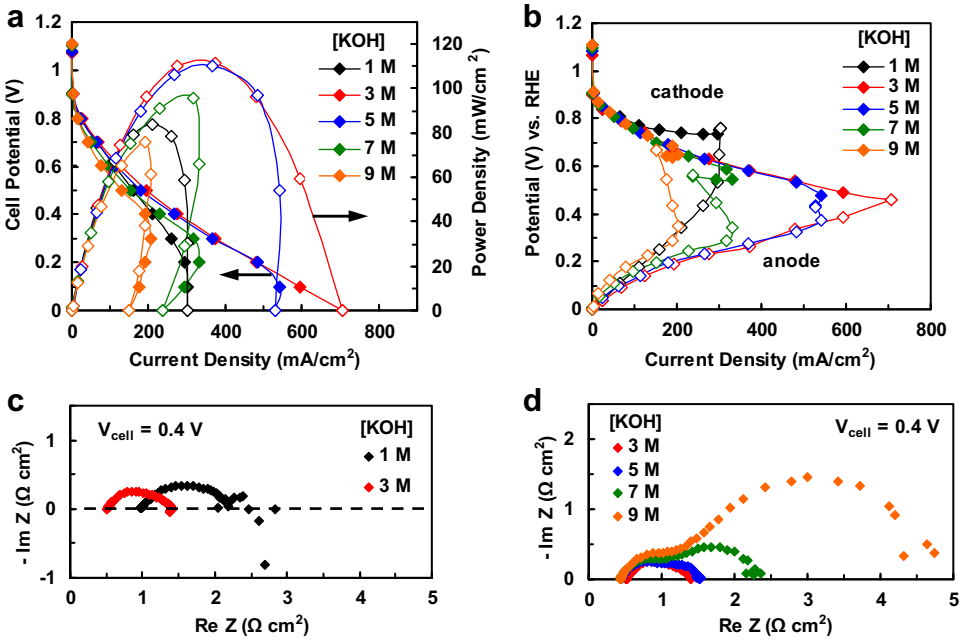

Fig. 5 – (a) Polarization and power density curves of alkaline microfluidic H_2/O_2 fuel cell as a function of KOH concentration; (b) Corresponding polarization curves (HP cathode/non-HP anode). (c) and (d) EIS spectra of an alkaline microfluidic H_2/O_2 fuel cell at 0.4 V. In all studies, H_2/O_2 flow rates were 50 sccm each, electrode loadings were 2 mg Pt/C/cm^2 (1 mg Pt/cm^2), electrolyte flow rate was 0.3 mL/min and experiments were performed at room temperature.

Increased solution viscosity hampers the removal of formed water from the anode catalyst layer causing electrode flooding. Also, at high KOH concentrations, a slight inversion is observed in the polarization curves after mass transport limitations are reached at low cell potentials ($V_{cell} \leq 0.2$ V). This inversion may be due to competitive hydroxyl absorption to the anode surface brought on by fuel-starvation conditions, caused by electrode flooding, and the highly concentrated electrolytes. This phenomenon is under further investigation and will be further discussed in a future publication. Furthermore, increasing kinetic limitations are observed at increased KOH concentrations due to competitive absorption of hydroxyl ions onto the electrode surface. Alcaide *et al.* observed similar competitive hydroxyl absorption effects at KOH $\geq$ 6 M when studying alkaline hydrogen oxidation on single Pt-based GDEs within a 3-electrode electrochemical cell [41]. Identical performance trends were observed with fuel cells operated with varying NaOH concentrations (not shown).

The effects of KOH concentrations on microfluidic fuel cell performance were further characterized via electrochemical impedance spectroscopy (EIS). EIS studies can be used to decouple the transport and electrochemical phenomena that govern the overall cell performance [31]. Previously, we have employed impedance analysis to investigate the performance of Ag/C cathodes, in a similar microfluidic configuration, as a function of KOH concentration (1, 3, and 5 M KOH) [24]. Fig. 5c and d shows the comparative Nyquist plots for the microfluidic H_2/O_2 fuel cell operated at 1, 3, 5, 7, and 9 M KOH. The R_{cell} values, the internal cell resistance, decrease with increasing electrolyte concentration, primarily due to reducing solution resistances, until a minimum value is reached at 7 M KOH. At 9 M KOH, solvation of the potassium ions reduces the number of free water molecules in solution, decreasing electrolyte conductivity [10]. Increasing the KOH concentration from 1 to 3 M KOH reduces the R_{ct} values, the charge-transfer resistance, as an increasing hydroxyl ion concentration improves catalytic activity (Fig. 5c). However, at KOH concentrations greater than 3 M, the adverse effects of anode flooding on hydrogen mass transport limitations appear as a low-frequency semi-circular feature impinging on the charge-transfer response (Fig. 5d).

While, optimal performance in this present microfluidic configuration is observed at 3 M KOH, the majority of AFCs with liquid electrolytes, both stationary and circulating, reported peak performance at ~7–8 M KOH [1,4,10,11]. However, these reported AFC technologies operate at elevated temperatures, $\geq$65 °C, which reduce electrolyte viscosity minimizing the adverse effects of flooding observed in the present room temperature studies. In fact, the solution viscosity of 8 M KOH at 65°C is near identical to that of 3 M KOH at room temperature [40]. Thus, for a room-temperature AFC with a liquid electrolyte, 3 M KOH appears to be the optimal electrolyte concentration. Note that further system-level studies to account for parasitic pumping losses and temperature effects are required to determine the feasibility of such room-temperature systems. In other work, we have employed a similar alkaline microfluidic fuel cell which is designed to more closely resemble an actual fuel cell-based power source (*i.e.*, air-breathing Ag-based cathode, low H_2 flow rate) [42].

3.4. *Utility of an alkaline microfluidic fuel cell for studying the effects of carbonate formation*

Independent control of electrolyte composition provides a means by which contaminant species can be introduced into the alkaline microfluidic H_2/O_2 fuel cell. This feature enables systematic analysis of the impact of contaminant species on individual electrode performance characteristics within an operating fuel cell. Of particular importance to viability of liquid- and membrane-based AFC technologies are the effects of carbonate formation on the electrode and in the electrolyte stream or polymeric AAEM (detailed in the Introduction). Flowing electrolyte-based AFCs are more carbonate tolerant than stagnant electrolyte-based AFCs because carbonate precipitation is dependent on saturation of the total electrolyte volume rather than the local electrolyte composition [9]. Thus, like in AAEM-based fuel cells, only carbonate ions impact the short-term performance of the flowing electrolyte-based AFCs. Introducing carbonate species into the electrolyte stream enables the analysis of the effects of carbonate ions on cell performance without the coupled effect of carbonate precipitation. To verify that the electrolyte could remove and/or prevent carbonate precipitation, we performed two proof-of-concept experiments where carbonate formation was triggered by gaseous CO_2 poisoning (Fig. 6).

In the first study, the ability of the flowing electrolyte stream to remove previously-formed carbonate species was investigated (Fig. 6a and b). In these studies, neat CO_2 was introduced on the anode side of a microfluidic H_2/O_2 fuel cell with a stationary 3 M KOH electrolyte. First, the cell performance is analyzed prior to CO_2 exposure to determine a baseline. Second, with the fuel cell off but not disassembled, pure CO_2 (15 sccm) flows over the anode for 10 min while N_2 (15 sccm) flows over the cathode. After the exposure, the microfluidic H_2/O_2 fuel cell is tested to determine any changes in performance. Third, a second 10 min CO_2 exposure and subsequent fuel cell test are performed without cell disassembly. Fourth, a 10 min KOH rinse is performed by flowing electrolyte, at 0.3 mL/min, through the microfluidic chamber. After this rinse, cell performance is tested, with a stationary electrolyte, to determine the effect of the KOH rinse.

Fig. 6a shows the polarization and power density curves of the microfluidic fuel cell, operating with a stationary 3 M KOH electrolyte, during this protocol. Exposure to CO_2 leads to significant performance losses as peak power density decreases from 102 to 31 mW/cm^2 after the first exposure (10 min total exposure) and then drops to 16 mW/cm^2 after the second exposure (20 min total exposure). However, after the KOH rinse, full peak power density of 103 mW/cm^2 is regained. In Fig. 6b, individual electrode polarization curves indicate that the carbonate species impact the anode performance while the cathode performance appears unaffected by the exposure. After the KOH rinse, anode performance is fully restored. The slight reduction in the maximum current density observed in the recovery data can be attributed to the few remaining precipitants that would most likely to be flushed away by a longer KOH rinse. Thus, the flowing electrolyte stream is an effective means of removing formed carbonates (both ions and precipitants) from the microfluidic AFC.

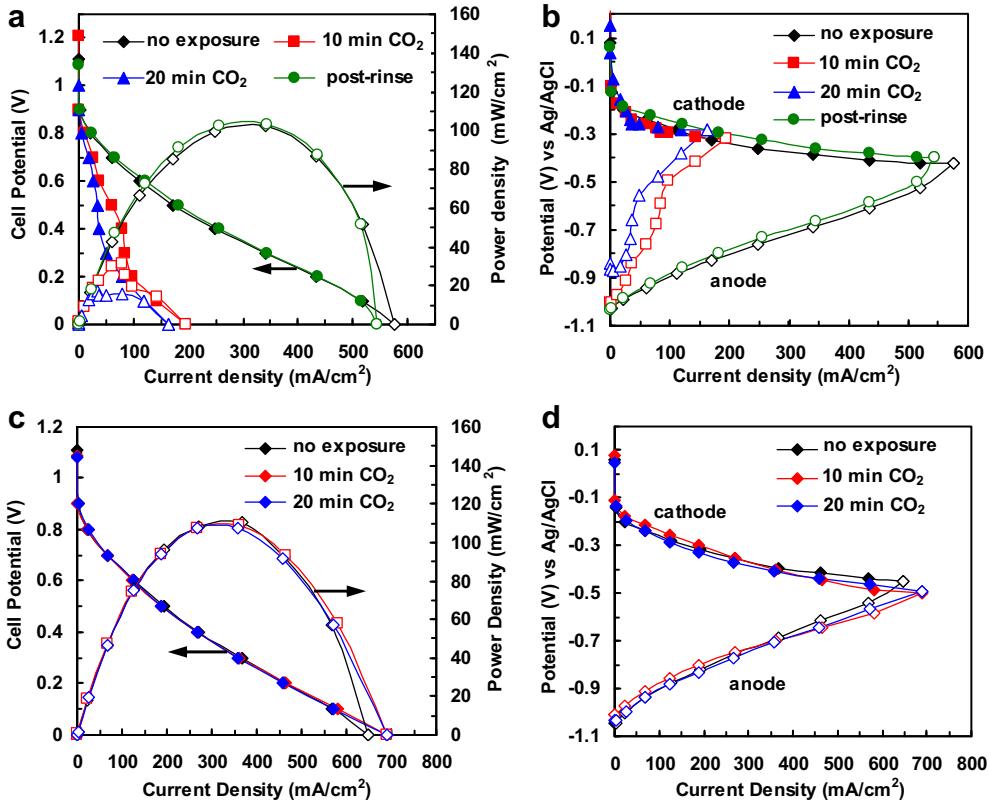

Fig. 6 – (a) Polarization and power density curves and (b) Corresponding anode and cathode polarization curves of the alkaline microfluidic H_2/O_2 fuel cell operated with a stationary electrolyte and exposed to CO_2. (c) Polarization and power density curves and (d) Corresponding anode and cathode polarization curves of the fuel cell operated with a flowing electrolyte and exposed to CO_2. In all studies, H_2/O_2 flow rates were 50 sccm each, electrode loadings were 2 mg Pt/C/cm^2 (1 mg Pt/cm^2), and experiments were performed at room temperature.

In the second study, the ability of the flowing electrolyte stream to prevent carbonate precipitation was investigated (Fig. 6c and d). In these studies, neat CO_2 was introduced on the anode side of a microfluidic H_2/O_2 fuel cell with a flowing 3 M KOH electrolyte at a flow rate of 0.3 mL/min. First, the cell performance is analyzed prior to CO_2 exposure to determine a baseline. Second, with the fuel cell off but not disassembled, pure CO_2 (15 sccm) flows over the anode for 10 min while N_2 (15 sccm) flows over the cathode. After the exposure, the microfluidic H_2/O_2 fuel cell is tested to determine any changes in performance. Third, the cell is exposed for 10 min to CO_2 for a second time and subsequent fuel cell tests are performed without cell disassembly.

The polarization and power density curves shown in Fig. 6c indicate that, with a flowing electrolyte, the microfluidic fuel cell performance is unaffected by exposure to CO_2 as any carbonates formed at the three-phase interface are immediately removed as long as the carbonates remain soluble in electrolyte solution. The individual electrode polarization curves confirm that both anode and cathode performance are unaffected by the exposure (Fig. 6d).

In summary, these two studies show that the flowing electrolyte stream can be used to prevent carbonate precipitation onto the electrode surface and thus enable the impact of soluble carbonate ions to be independently observed. Consequently, this microfluidic configuration can be used to investigate the impact of carbonates on electrode performances for both liquid electrolyte- and AAEM-based fuel cells.

3.5. *Effects of carbonates on electrode performance*

By employing the microfluidic platform used in this study, carbonate poisoning in an AFC can be simulated by systematically varying the composition of the electrolyte stream. Fig. 7 shows the effects of increasing carbonate poisoning on individual electrode and overall cell performance upon stoichiometrically replacing KOH with K_2CO_3 in increments of 0.5 M KOH, starting with 3 M KOH (Table 2). Fig. 7a shows polarization and power density curves for the microfluidic H_2/O_2 fuel cell operating with a flowing electrolyte of varying composition. Note that the individual electrode curves shown in Fig. 7b are qualitatively similar to those observed in Fig. 6b indicating the effectiveness of this analytical method in simulating carbonate poisoning.

Carbonate poisoning in the electrolyte significantly lowers fuel cell performance due to significant limitations in anodic processes (Fig. 7b). As carbonate concentration is increased (and hydroxyl concentration decreased) the anode performance lowers and a potential-dependent feature is observed around −0.65 V vs. Ag/AgCl in solutions B, C, and D. As the

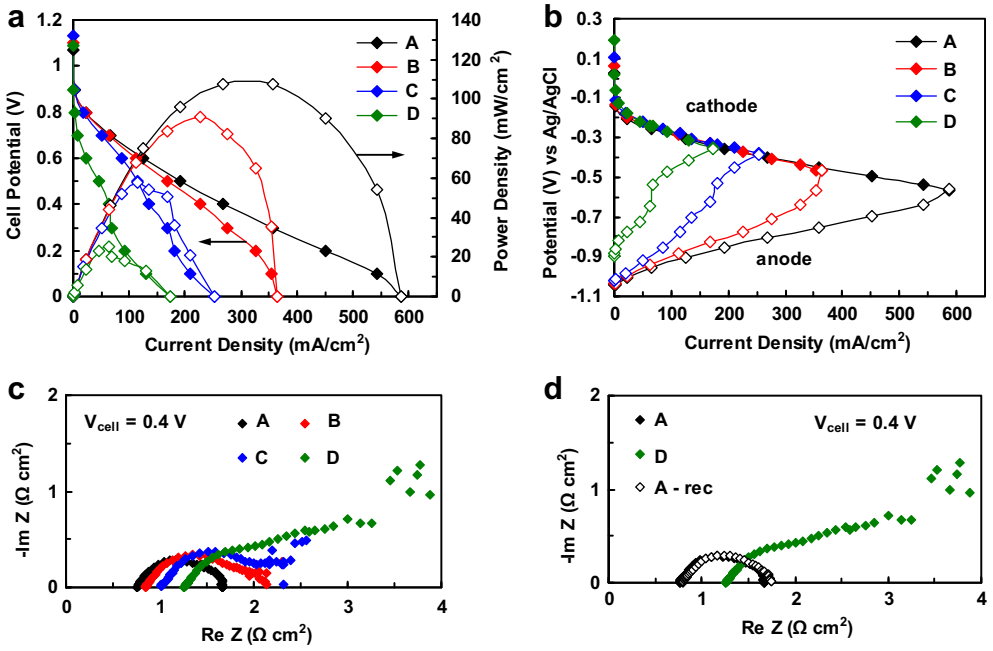

Fig. 7 – (a) Polarization and power density curves of alkaline microfluidic H_2/O_2 fuel cell as a function of carbonate content in the electrolyte stream; (b) Corresponding anode and cathode polarization curves. Nyquist plots of the alkaline microfluidic H_2/O_2 fuel cell show (c) the effects of carbonate content and (d) the process reversibility. In all studies, H_2/O_2 flow rates were 50 sccm each, electrode loadings were 2 mg Pt/C/cm^2 (1 mg Pt/cm^2), electrolyte flow rate was 0.3 mL/min, and experiments were performed at room temperature.

carbonate ions are negatively charged species, they migrate toward the anode surface increasing local carbonate concentrations, decreasing the hydroxyl ion concentration, and lowering pH [17]. Indeed, in the case where the microfluidic fuel cell is operated with the carbonate-only solution (D in Fig. 7), the open circuit anode potential shifts upwards as compared to operation with the other solutions (A–C) due to the pH shift. However, even in a carbonate-only electrolyte, (D in Fig. 7) the microfluidic fuel cell continued to operate which indicate that carbonate poisoning reduces but does not completely eliminate the fuel cell performance. These observations are in good agreement with recent AAEM-based fuel cell literature [14,15,17]. Notably, Yanagi et al. demonstrated a CO_2 self-purging mechanism at the anode through power generation where carbonate species could be removed from the AAEM and exit the fuel cell anode outlet as CO_2 [15]. However, others have observed that not only can AAEM-based fuel cells operate using a carbonate cycle, as opposed to hydroxyl cycle, but that these systems can also outperform their hydroxyl-based counterparts [42,43]. Recently, Vega et al. proposed a hydrogen oxidation pathway which proceeds directly through carbonates and is thermodynamically more favorable than an equivalent hydroxyl-based reaction pathway [44]. However, the carbonate-based hydrogen oxidation reaction occurs at a higher onset potential than the hydroxyl-based reaction. Thus in a mixed electrolyte (hydroxyls and carbonates) the performance decreases with increasing carbonate concentration (decreasing hydroxyl concentration) which indicates that carbonates hamper anode performance. However, at high anode potentials a shift appears to occur which may be related to the onset of the carbonate pathway. This potential dependent onset may explain the anode curves observed for fuel cells operated in solutions B, C, and D. Note that even in carbonate-only electrolyte (solution D) hydroxyl ions are generated on the cathode. On the cathode side, the generation of negatively charged hydroxyl ions not only prevents carbonates from traveling to that surface but also maintains a high local pH. Consequently, the cathode performance in Fig. 7b, like in Fig. 6b, appears to be independent of carbonate concentration. These results are further supported by recent observations in a 3-electrode electrochemical cell as reported by Vega and Mustain [43].

Table 2 – Legend for the [KOH]: [K_2CO_3] ratio studies shown in Fig. 7.

Legend	[KOH]: [K_2CO_3] (M: M)
A/A-rec	3: 0
B	2: 0.5
C	1: 1
D	0: 1.5

Fig. 7c and d show impedance spectra of the microfluidic H_2/O_2 fuel cell operated with varying alkaline electrolyte compositions (KOH: K_2CO_3 ratios). With increasing carbonate concentrations, R_{cell} increases indicating reduced electrolyte conductivity, which can be expected due to the lowered hydroxyl ion concentrations. The shape of the semi-circular Nyquist features also varies with increasing carbonate concentrations. The fuel cell spectra shifts from a surface

reaction-limited process, as indicated by the "closed" semi-circular feature (curve A), to a transport-limited process, as indicated by the "open" mass transfer slope (curve D) with increased carbonate concentration [31]. This shift can be attributed to increased carbonate concentrations in close proximity to the anodic catalytic sites which hinder hydroxyl ion transport. Furthermore, impedance analysis shows that these effects are reversible as changing the dynamic electrolyte composition from pure KOH (curve A) to pure K_2CO_3 (curve D), and back to pure KOH (curve A-rec) and (curve D) solutions, again indicating that no carbonate species precipitate (Fig. 7d).

These carbonate studies highlight the utility of the microfluidic fuel cell used here as an analytical platform for measuring contaminant effects on individual electrode and overall cell performance. In a separate study, we performed extensive studies of the critical parameters (*i.e.,* concentrations, exposure time) that govern the impact of carbonate species on air-breathing AFC performance and lifetime [42]. Indeed, beyond carbonates, similar techniques may be employed to rapidly characterize the effects of a broad range of contaminants (*e.g.*, unreacted organic fuels, by-products of incomplete fuel reformation, airborne pollutants) on the individual electrode and overall cell performance of both alkaline and acidic fuel cell systems [2].

4. Conclusions

With renewed interest in AFC systems, a need exists for a more detailed understanding and subsequent optimization of electrode performance as a function of preparation methods and operating parameters for the development of robust and cost-effective power sources. A microfluidic H_2/O_2 fuel cell is a convenient and powerful platform for probing the underlying processes that govern the performance of electrodes within a working fuel cell. We performed detailed analyses of Pt/C-based electrode performance as a function of preparation procedures and fuel cell operating parameters. Our studies demonstrate that in hydrogen-fueled AFCs, *unlike in their acidic counterparts*, transport processes to and from the anode significantly contribute to polarization losses and often limit performance. In fact, an AFC anode is more similar to an acidic fuel cell cathode since both must efficiently remove generated water to maintain performance. Our studies indicate that AFC anode performance is a strong function of both electrode structure (*i.e.,* compression, hydrophobicity) and electrolyte properties (*i.e.*, conductivity, viscosity). In contrast, the AFC cathode performance appears independent of both structure and electrolyte properties.

We also present a useful technique for studying the effects of contaminant species, here carbonates, on individual electrode and fuel cell performance. Cell performance is unaffected by carbonate formation if the cell is subsequently rinsed with fresh electrolyte. The anode performance is limited by the presence of carbonate species due to reduced local pH and blocking hydroxyl transport to the electrocatalytic sites. The cathode performance is unaffected by the presence of carbonate species as the generation of negatively-charged hydroxyl ions not only prevents carbonates from traveling to that surface but also maintains a high local pH.

While continued research into improving cathode performance remains critical, these observations suggest that significant efforts must also be focused developing novel anode materials for AFC applications. Electrode materials and structures must be designed that improve water management and limit performance degradation. Furthermore, Pt-free anode electrocatalysts (*i.e.*, Ni-based materials) must be developed that operate efficiently at lower alkaline pH and in the presence of carbonate species to create more robust fuel cell-based power sources.

Acknowledgments

We gratefully acknowledge financial support from the National Science Foundation (Career Grant CTS 05-47617), the Department of Energy (Grant DEFG02005ER46260), the Army Research Office (Grant W911NF-10-2-0054) and a GEM Fellowship for FRB. The MicroCT experiments were performed at in the Microscopy Suite of the Imaging Technology Group in the Beckman Institute. We acknowledge Darren Stevenson for his assistance performing the MicroCT analyses. We are grateful to Dr. Wei-Ping Zhou, Dr. John Haan, and Molly Jhong for stimulating discussions. We are also grateful to Joshua Tice and Sudipto Guha for help with preparing figures.

REFERENCES

[1] Carrette L, Friedrich KA, Stimming U. Fuel cells: principles, types, fuels, and applications. ChemPhysChem 2000;4:162–93.
[2] Borup R, Meyers J, Pivovar B, Kim YS, Mukundan R, Garland N, et al. Scientific aspects of polymer electrolyte fuel cell durability and degradation. Chem Rev 2007;10:3904–51.
[3] Spendelow JS, Wieckowski A. Electrocatalysis of oxygen reduction and small alcohol oxidation in alkaline media. Phys Chem Chem Phys 2007;21:2654–75.
[4] Gouerec P, Poletto L, Denizot J, Sanchez-Cortezon E, Miners JH. The evolution of the performance of alkaline fuel cells with circulating electrolyte. J Power Sources 2004;2:193–204.
[5] Gülzow E. Alkaline fuel cells. Fuel Cells 2004;4:251–5.
[6] McLean GF, Niet T, Prince-Richard S, Djilali N. An assessment of alkaline fuel cell technology. Int J Hydrog Energy 2002;5:507–26.
[7] Perry ML, Fuller TF. A historical perspective of fuel cell technology in the 20th century. J Electrochem Soc 2002;7:S59–67.
[8] Kordesch K, Gsellmann J, Cifrain M, Voss S, Hacker V, Aronson RR, et al. Intermittent use of a low-cost alkaline fuel cell-hybrid system for electric vehicles. J Power Sources 1999;1-2:190–7.
[9] Cifrain M, Kordesch KV. Advances, aging mechanism and lifetime in AFCs with circulating electrolytes. J Power Sources; 2004:234–42.
[10] Lin BYS, Kirk DW, Thorpe SJ. Performance of alkaline fuel cells: a possible future energy system? J Power Sources 2006;1:474–83.
[11] Burchardt T, Gouerec P, Sanchez-Cortezon E, Karichev Z, Miners JH. Alkaline fuel cells: contemporary advancement and limitations. Fuel; 2002:2151–5.

[12] Koscher GA, Kordesch K. Alkaline methanol-air system - A historical survey and some new work. J Solid State Electrochem 2003;9:632–6.
[13] Varcoe JR, Slade RCT. Prospects for alkaline anion-exchange membranes in low temperature fuel cells. Fuel Cells 2005;2: 187–200.
[14] Adams LA, Poynton SD, Tamain C, Slade RCT, Varcoe JR. A carbon dioxide tolerant aqueous-electrolyte-free anion-exchange membrane alkaline fuel cell. ChemSusChem 2008; 1-2:79–81.
[15] Yanagi H, Fukuta K. Anion exchange membrane and Ionomer for alkaline membrane fuel cells (AMFCs). ECS Trans 2008;2:257–62.
[16] Lu SF, Pan J, Huang AB, Zhuang L, Lu JT. Alkaline polymer electrolyte fuel cells completely free from noble metal catalysts. Proc Natl Acad Sci U S A 2008;52:20611–4.
[17] Wang Y, Li L, Hu L, Zhuang L, Lu JT, Xu BQ. A feasibility analysis for alkaline membrane direct methanol fuel cell: thermodynamic disadvantages versus kinetic advantages. Electrochem Commun 2003;8:662–6.
[18] Varcoe JR, Slade RCT, Yee E Lam How. An alkaline polymer electrochemical interface: a breakthrough in application of alkaline anion-exchange membranes in fuel cells. Chem Commun 2006;13:1428–9.
[19] Varcoe JR, Slade RCT, Wright GL, Chen YL. Steady-state dc and impedance investigations of H_2/O_2 alkaline membrane fuel cells with commercial Pt/C, Ag/C, and Au/C cathodes. J Phys Chem B 2006;42:21041–9.
[20] Kucernak AR, Toyoda E. Studying the oxygen reduction and hydrogen oxidation reactions under realistic fuel cell conditions. 2008;11:1728–1731.
[21] Hizir FE, Ural SO, Kumbur EC, Mench MM. Characterization of interfacial morphology in polymer electrolyte fuel cells: micro-porous layer and catalyst layer surfaces. J Power Sources 2010;11:3463–71.
[22] Kim S, Khandelwal M, Chacko C, Mench MM. Investigation of the impact of interfacial delamination on polymer electrolyte fuel cell performance. 2009;1:B99–B108.
[23] Ramasamy RP, Kumbur EC, Mench MM, Liu W, Moore D, Murthy M. Investigation of macro- and micro-porous layer interaction in polymer electrolyte fuel cells. 2008;13:3351–3367.
[24] Brushett FR, Zhou WP, Jayashree RS, Kenis PJA. Alkaline microfluidic hydrogen-oxygen fuel cell as a cathode characterization platform. J Electrochem Soc 2009;5: B565–71.
[25] Jayashree RS, Mitchell M, Natarajan D, Markoski LJ, Kenis PJA. Microfluidic hydrogen fuel cell with a liquid electrolyte. Langmuir 2007;13:6871–4.
[26] Brushett FR, Duong HT, Ng JWD, Wieckowski A, Kenis PJA. Investigation of Pt, Pt_3Co and Pt_3Co/Mo cathodes for the oxygen reduction reaction in an acidic microfluidic H_2/O_2 fuel cell. J Electrochem Soc 2010;6:B837–45.
[27] Choban ER, Waszczuk P, Kenis PJA. Characterization of limiting factors in laminar flow-based membraneless microfuel cells. Electrochem Solid State Lett 2005;7: A348–52.
[28] Fluckiger R, Freunberger SA, Kramer D, Wokaun A, Scherer GG, Buchi FN. Anisotropic, effective diffusivity of porous gas diffusion layer materials for PEFC. Electrochim Acta; 2008:551–9.
[29] Ghouse M, Alboeiz A, Abaoud H, Algarni M. Preparation and evaluation of PTFE-bonded porous gas-diffusion carbon electrodes use in phosphoric-acid fuel cell applications. Int J Hydrog Energy 1995;9:727–36.
[30] Stock SR. Microcomputed tomography: methodology and applications. Boca Raton: CRC Press; 2009.
[31] Bard AJ, Faulkner LR. Electrochemical methods: fundamentals and applications. 2nd. Hoboken: John Wiley & Sons, Inc; 2001.
[32] Freire TJP, Gonzalez ER. Effect of membrane characteristics and humidification conditions on the impedance response of polymer electrolyte fuel cells. J Electroanal Chem 2001;1-2: 57–68.
[33] Frey T, Linardi M. Effects of membrane electrode assembly preparation on the polymer electrolyte membrane fuel cell performance. Electrochim Acta; 2004:99–105.
[34] Prasanna M, Cho EA, Lim T-H, Oh I-H. Effects of MEA fabrication method on durability of polymer electrolyte membrane fuel cells. Electrochim Acta; 2008:5434–41.
[35] Srinivasan S. Fuel cells. From fundamentals to applications. New York: Springer; 2006.
[36] Zeng R, Poynton SD, Kizewski JP, Slade RCT, Varcoe JR. A novel reference electrode for application in alkaline polymer electrolyte membrane fuel cells. Electrochem Commun 2010;6:823–5.
[37] Gasteiger HA, Kocha SS, Sompalli B, Wagner FT. Activity benchmarks and requirements for Pt, Pt-alloy, and non-Pt oxygen reduction catalysts for PEMFCs. Appl Catal. B 2005;1-2:9–35.
[38] Lee WK, Ho CH, Van Zee JW, Murthy M. The effects of compression and gas diffusion layers on the performance of a PEM fuel cell. J Power Sources 1999;1:45–51.
[39] Bazylak A, Sinton D, Liu ZS, Djilali N. Effect of compression on liquid water transport and microstructure of PEMFC gas diffusion layers. J Power Sources 2007;2:784–92.
[40] Olin Chlor Alkali Products, http://koh.olinchloralkali.com/TechnicalInformation/default.aspx; September 25, 2009.
[41] Alcaide F, Brillas E, Cabot PL. Hydrogen oxidation reaction in a Pt-catalyzed gas diffusion electrode in alkaline medium. J Electrochem Soc 2005;10:E319–27.
[42] Naughton MS, Brushett FR, Kenis PJA. Carbonate Resilience of a flowing electrolyte alkaline fuel cells. J Power Sources 2010;4:1762–8.
[43] Vega JA, Mustain WE. Effect of CO_2, HCO_3^- and CO_3^{-2} on oxygen reduction in anion exchange membrane fuel cells. Electrochim Acta 2010;5:1638–44.
[44] Vega JA, Smith S, Mustain WE. Hydrogen and methanol oxidation reaction in hydroxide and carbonate alkaline media. J Electrochem Soc 2011;4:B349–54.